Springer Earth System Sciences

Andrés Folguera
Maximiliano Naipauer
Lucía Sagripanti
Matías C. Ghiglione
Darío L. Orts
Laura Giambiagi *Editors*

Growth of the Southern Andes

Springer

Springer Earth System Sciences

More information about this series at http://www.springer.com/series/10178

Andrés Folguera · Maximiliano Naipauer
Lucía Sagripanti · Matías C. Ghiglione
Darío L. Orts · Laura Giambiagi
Editors

Growth of the Southern Andes

Springer

Editors
Andrés Folguera
Departamento de Ciencias Geológicas,
Facultad de Ciencias Exactas y Naturales
Instituto de Estudios Andinos "Don Pablo
Groeber" UBA-CONICET
Buenos Aires
Argentina

Maximiliano Naipauer
Departamento de Ciencias Geológicas,
Facultad de Ciencias Exactas y Naturales
Instituto de Estudios Andinos "Don Pablo
Groeber" UBA-CONICET
Buenos Aires
Argentina

Lucía Sagripanti
Departamento de Ciencias Geológicas,
Facultad de Ciencias Exactas y Naturales
Instituto de Estudios Andinos "Don Pablo
Groeber" UBA-CONICET
Buenos Aires
Argentina

Matías C. Ghiglione
Departamento de Ciencias Geológicas,
Facultad de Ciencias Exactas y Naturales
Instituto de Estudios Andinos "Don Pablo
Groeber" UBA-CONICET
Buenos Aires
Argentina

Darío L. Orts
Instituto de Investigación en Paleobiología
y Geología, Universidad Nacional
de Río Negro—CONICET
General Roca (Río Negro)
Argentina

Laura Giambiagi
Centro Regional de Investigaciones
Científicas y Tecnológicas
IANIGLA, CCT Mendoza
Mendoza
Argentina

ISSN 2197-9596 ISSN 2197-960X (electronic)
Springer Earth System Sciences
ISBN 978-3-319-23059-7 ISBN 978-3-319-23060-3 (eBook)
DOI 10.1007/978-3-319-23060-3

Library of Congress Control Number: 2015954348

Springer Cham Heidelberg New York Dordrecht London

Printed on acid-free paper

Springer International Publishing AG Switzerland is part of Springer Science+Business Media (www.springer.com)

Contents

Contributors

Orlando Álvarez Instituto Geofísico y Sismológico Ing. Volponi, Universidad Nacional de San Juan, San Juan, Argentina; Consejo Nacional de Investigaciones Cientifícas y Técnicas (CONICET), Buenos Aires, Argentina

Vanesa Barberón Departamento de Ciencias Geológicas, Facultad de Ciencias Exactas y Naturales, Instituto de Estudios Andinos "Don Pablo Groeber" UBA-CONICET, Buenos Aires, Argentina

Florencia Bechis IIDyPCa, CONICET, Universidad Nacional de Río Negro, San Carlos de Bariloche, Argentina

Germán Bottesi Gerencia de desarrollo de no convencionales, YPF S.A., Capital Federal, Argentina

Francisco Chiachiarelli Desarrollo, YPF S.A., Neuquén, Argentina

José Cuitiño Departamento de Ciencias Geológicas, Facultad de Ciencias Exactas y Naturales, Instituto de Geociencias Básicas, Aplicadas y Ambientales (IGEBA) UBA-CONICET, Buenos Aires, Argentina

Rafael Toural Dapoza Centro Regional de Investigaciones Científicas y Tecnológicas, IANIGLA, CCT Mendoza, Mendoza, Argentina

Andrés Echaurren Departamento de Ciencias Geológicas, Facultad de Ciencias Exactas y Naturales, Instituto de Estudios Andinos "Don Pablo Groeber" UBA-CONICET, Buenos Aires, Argentina

Alfonso Encinas Departamento de Ciencias de la Tierra, Universidad de Concepción, Concepción, Chile

Lucas Fennell Departamento de Ciencias Geológicas, Facultad de Ciencias Exactas y Naturales, Instituto de Estudios Andinos "Don Pablo Groeber" UBA-CONICET, Buenos Aires, Argentina

Alicia Folguera SEGEMAR, Buenos Aires, Argentina

Andrés Folguera Departamento de Ciencias Geológicas, Facultad de Ciencias Exactas y Naturales, Instituto de Estudios Andinos “Don Pablo Groeber” UBA-CONICET, Buenos Aires, Argentina

Matías C. Ghiglione Departamento de Ciencias Geológicas, Facultad de Ciencias Exactas y Naturales, Instituto de Estudios Andinos “Don Pablo Groeber” UBA-CONICET, Buenos Aires, Argentina

Laura Giambiagi Centro Regional de Investigaciones Científicas y Tecnológicas, IANIGLA, CCT Mendoza, Mendoza, Argentina

Guido Gianni Departamento de Ciencias Geológicas, Facultad de Ciencias Exactas y Naturales, Instituto de Estudios Andinos “Don Pablo Groeber” UBA-CONICET, Buenos Aires, Argentina

Mario Gimenez Instituto Geofísico y Sismológico Ing. Volponi, Universidad Nacional de San Juan, San Juan, Argentina; Consejo Nacional de Investigaciones Cientifícas y Técnicas (CONICET), Buenos Aires, Argentina

Gregory Hoke Department of Earth Sciences, Syracuse University, Syracuse, NY, USA

Federico Lince Klinger Instituto Geofísico y Sismológico Ing. Volponi, Universidad Nacional de San Juan, San Juan, Argentina; Consejo Nacional de Investigaciones Cientifícas y Técnicas (CONICET), Buenos Aires, Argentina

Ana Lossada Centro Regional de Investigaciones Científicas y Tecnológicas, IANIGLA, CCT Mendoza, Mendoza, Argentina

Diego Mardonez CONICET, Universidad Nacional de San Luis, San Luis, Argentina

Patricia Martinez Instituto Geofísico y Sismológico Ing. Volponi, Universidad Nacional de San Juan, San Juan, Argentina; Consejo Nacional de Investigaciones Cientifícas y Técnicas (CONICET), Buenos Aires, Argentina

Manuela Mazzitelli CONICET, Universidad Nacional de San Luis, San Luis, Argentina

José Mescua Centro Regional de Investigaciones Científicas y Tecnológicas, IANIGLA, CCT Mendoza, Mendoza, Argentina

Stella Maris Moreiras Centro Regional de Investigaciones Científicas y Tecnológicas, IANIGLA, CCT Mendoza, Mendoza, Argentina

Maximiliano Naipauer Departamento de Ciencias Geológicas, Facultad de Ciencias Exactas y Naturales, Instituto de Estudios Andinos “Don Pablo Groeber” UBA-CONICET, Buenos Aires, Argentina

César Navarrete Departamento de Geología, F.C.N., Universidad Nacional de la Patagonia “San Juan Bosco”, YPF, Santo Domingo, Argentina

Darío L. Orts Instituto de Investigación en Paleobiología y Geología, Universidad Nacional de Río Negro—CONICET, General Roca (Río Negro), Argentina

Diego Sebastián Pagano CONICET, Universidad Nacional de San Luis, San Luis, Argentina

Miguel E. Ramos Departamento de Ciencias Geológicas, Facultad de Ciencias Exactas y Naturales, Instituto de Estudios Andinos "Don Pablo Groeber" UBA-CONICET, Buenos Aires, Argentina

Victor A. Ramos Departamento de Ciencias Geológicas, Facultad de Ciencias Exactas y Naturales, Instituto de Estudios Andinos "Don Pablo Groeber" UBA-CONICET, Buenos Aires, Argentina

Emilio Agustín Rojas Vera Departamento de Ciencias Geológicas, Facultad de Ciencias Exactas y Naturales, Instituto de Estudios Andinos "Don Pablo Groeber" UBA-CONICET, Buenos Aires, Argentina

Francisco Ruiz Instituto Geofísico y Sismológico Ing. Volponi, Universidad Nacional de San Juan, San Juan, Argentina

Lucía Sagripanti Departamento de Ciencias Geológicas, Facultad de Ciencias Exactas y Naturales, Instituto de Estudios Andinos "Don Pablo Groeber" UBA-CONICET, Buenos Aires, Argentina

Silvana Spagnotto Departamento de Física, Universidad Nacional de San Luis, San Luis, Argentina

Julieta Suriano Departamento de Ciencias Geológicas, Facultad de Ciencias Exactas y Naturales, Instituto de Geociencias Básicas, Aplicadas y Ambientales (IGEBA) UBA-CONICET, Buenos Aires, Argentina

Gonzalo Zamora Valcarce Complex Tectonics, Repsol S.A, Houston, TX, USA

An Introduction to the Southern Andes (33–50°S): Book Structure

Andrés Folguera, Maximiliano Naipauer, Lucía Sagripanti, Matías C. Ghiglione, Darío L. Orts and Laura Giambiagi

1 Introduction

This book intends to constitute a useful tool to access to data and a general discussion about the mechanisms that have been associated with the development of the Southern Andes. It is mainly conceived for Earth Science professionals working in academia and industry, as well as Ph.D and Ms students and interested readers in general.

This book is structured through a total number of 11 chapters, where the initial three are focused on general aspects such as crustal density structure and main source areas of the sedimentary basins that characterize the Southern Andes through time, while the other eight analyze the structure and evolution of particular

A. Folguera (✉) · M. Naipauer · L. Sagripanti · M.C. Ghiglione
Departamento de Ciencias Geológicas, Facultad de Ciencias Exactas y Naturales, Instituto de Estudios Andinos "Don Pablo Groeber" UBA-CONICET, Buenos Aires, Argentina
e-mail: andresfolguera2@yahoo.com.ar

M. Naipauer
e-mail: maxinaipauer@gl.fcen.uba.ar

L. Sagripanti
e-mail: lusagripanti@gmail.com

M.C. Ghiglione
e-mail: mcghiglione@gmail.com

D.L. Orts
Instituto de Investigación en Paleobiología y Geología, Universidad Nacional de Río Negro—CONICET, General Roca (Río Negro), Argentina
e-mail: dlorts@yahoo.com

L. Giambiagi
Centro Regional de Investigaciones Científicas y Tecnológicas, IANIGLA, CCT Mendoza, Mendoza, Argentina
e-mail: lgiambia@mendoza-conicet.gob.ar

A. Folguera et al. (eds.), *Growth of the Southern Andes*,
Springer Earth System Sciences, DOI 10.1007/978-3-319-23060-3_1

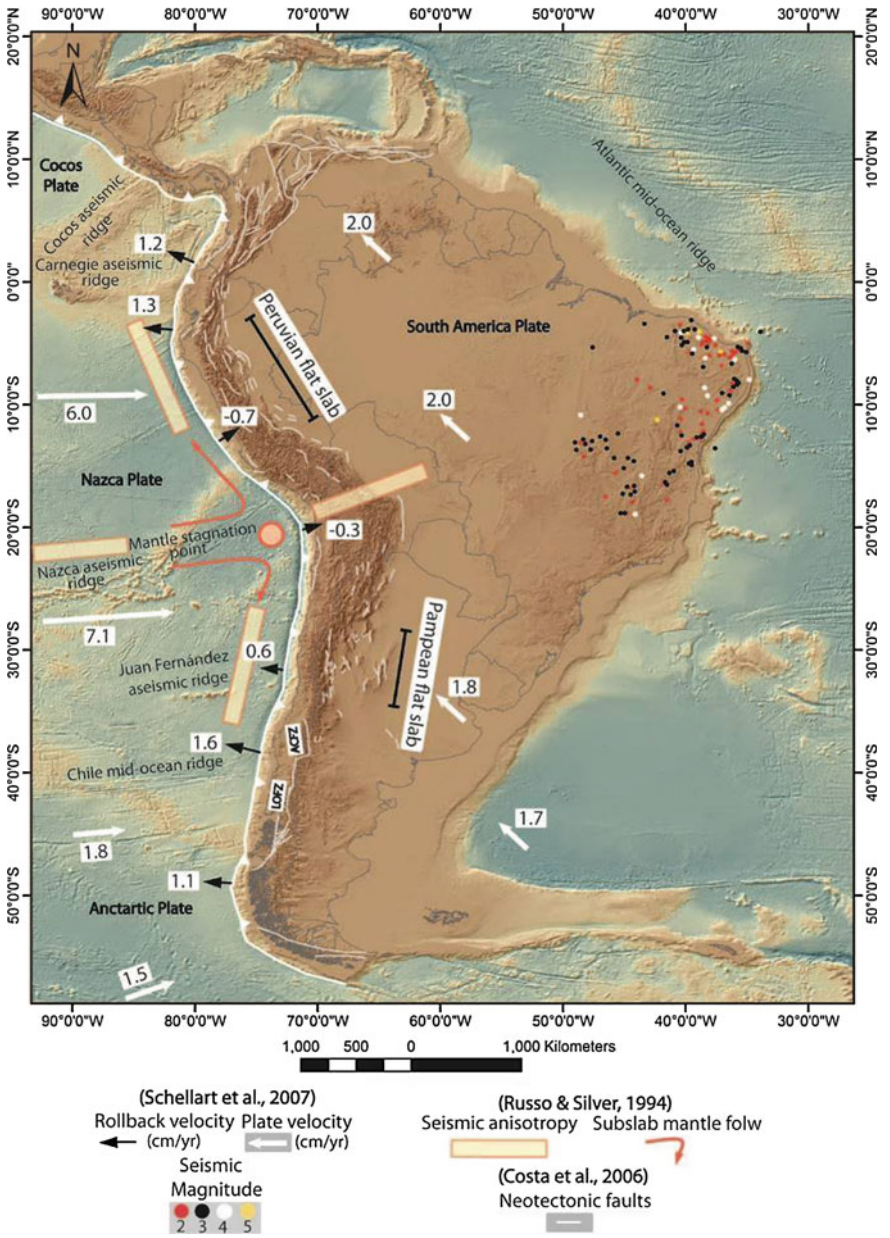

Fig. 1 The Andes, considered the product of subduction of a series of Pacific plates, have a peculiar symmetrical geometry that has been noted and analyzed in different studies. This is characterized by (i) a central plateau bordered by sub-Andean systems, (ii) north and south of it two flat slabs where deformation progressed into the foreland area as thick-skinned broad domains, (iii) two sectors north and south respectively characterized by lower elevations and narrower amplitudes and finally (iv) two transform plate boundaries that separate the South American Plate from two smaller plates. This work is focused in the area located south of the southern flat slab non formally denominated Southern Andes

mountain sectors ordered from north to south. The book contains maps, schemes and cross sections that constitute up-to-date proposals that use previous and new datasets. Different sources are cited at the end of each chapter that can be used to expand particular points discussed in the book.

The segment that is being analyzed in this book develops south of the Pampean flat subduction zone, one of the three flat subduction zones that affect western South America and one of the largest in the world (Fig. 1). We are referring to this segment with a non-formal denomination that is "Southern Andes" that comprises the sectors comprehended south of the Pampean flat subduction zone up to the southernmost tip of the continent (Fig. 1). This segment shows a marked fall in topography from the southern flat slab zone to the south as well as a reduction in amplitude and orogenic shortenings (Fig. 1). Schellart et al. (2007) have proposed a coherent frame to explain these morphostructural differences of the Andes along strike. The central part of the Andes coincides with the Arica bending and the broadest part of the mountain system (Fig. 1). This is explained by a stagnant asthenospheric zone produced between two divergent mantle flows west of the subduction zone of the Cocos, Nazca and Antarctic plates, revealed by mantle anisotropic studies (Russo and Silver 1994). This stagnant point would have determined a nearly stationary trench through time that is not able to retreat such as the two slab edges of the Andean subduction system, where parallel to the trench asthenospheric flows do not impede slab retreat (Fig. 1) (Schellart et al. 2007). According to Schellart et al. (2007), long subduction zones do not facilitate, and at a certain point difficult, interchange between asthenospheric compartments that are comprehended below and above the subducted slab, a process that usually occurs at subducted slab edges during slab retreat. This explains why westward displacement of the South American Plate that is imposed by the ridge push forces associated with the Atlantic Ridge is absorbed at the Arica bending latitudes as permanent deformation in the Subandean region flanking the Altiplano, and at a certain extent in the Bazilian coast as passive margin mountains (Fig. 1).

This book concentrates in the southern half of this system along a segment characterized by an important topographic gradient (Fig. 1). This constitutes a long term analysis trying to conceal and compare present morphology and acting processes with the initial stages of Andean development.

2 The Andean Segmentation

Several proposals for the Andean segmentation that attend different geological evolutions, magmatism, structure, subduction geometry and topography have been proposed, which differ substantially from each other (Fig. 2). The first classification of the Andes using plate tectonics criteria was proposed by Gansser (1973) who differentiated Northern, Central, and Southern Andes (Fig. 2a). According to this classification, the Northern Andes are developed between 10°N and 4°S, from their confluence with the Caribbean Andes to the point of inception of the Carnegie ridge

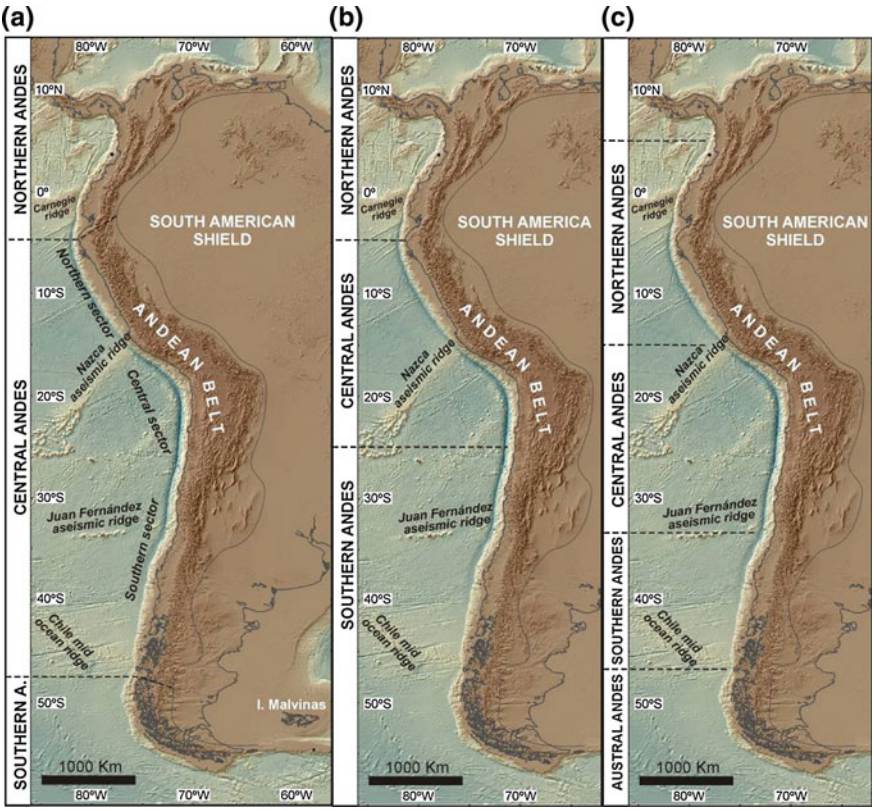

Fig. 2 Different Andean segmentation proposals according to: **a** Gansser (1973) and Ramos (1999) (*to the left*); **b** Auboin (1973) and Auboin et al. (1973) (*middle part*); **c** Tassara and Yáñez (2003) (*to the right*)

into the trench. These Andes are formed by a complex collage of different kinds of oceanic terranes mainly formed at the Galápagos hot spot that were incorporated into the accretionary wedge producing rapid expansion of the continental margin, deformation and metamorphism (see Ramos 2009 for a synthesis). The Central Andes to the south lie between 4°S and 46°30′S, between the Guayaquil Gulf and the Chile mid ocean ridge. The most striking characteristic of this long segment is that it has not experienced ocean crust accretions in Mesozoic and Cenozoic times, with a basement consolidated early since the Late Proterozoic and Early Paleozoic. Then no Mesozoic to Cenozoic metamorphic processes have affected the margin associated with collision of continental and oceanic fragments, with an evolution mainly linked to a subduction system (see Ramos 2009). The Southern Andes between 46°30′S and 52°S is again considered an accretionary orogen with the presence of metamorphic and oceanic rocks of Mesozoic age (Fig. 2a) (Gansser 1973). Ramos (1999, 2009, 2010; among others), following the classical segmentation of Gansser (1973),

introduced a subdivision of the Central Andes, mainly attending to changes in the Wadati-Benioff geometry, that comprehended northern (4°S–14°S), central (14°S–27°S), and southern sectors (27°S–46°30′S) (Fig. 2a).

Auboin (1973) divided the Andes in Northern, Central, and Southern (Fig. 2b). Even though this subdivision is based on geological features and paleogeography, topography, and involved orogenic cycles, it is contextualized in the geosynclinal model, reason by which this classification is presently discarded (Auboin et al. 1973).

Recently Tassara and Yáñez (2003) proposed a new subdivision, based on topography and factors inherent to the continental crust. Unlike the other two proposals, these authors divided the Andes in four segments: northern (5°N–15°S), central (15°S–33°30′S), southern (33°30′S–47°S), and austral (47°S–57°S) (Fig. 2c).

We use the informal name of "Southern Andes" for the segment south of 33°S that is the case study of this book, roughly equivalent to the Southern and Austral segments of Tassara and Yáñez (2003). This segment overlaps the southern sector of the Central and Southern Andes in terms of Gansser (1973) and Ramos (1999).

3 Morphostructural Provinces

The morphostructural Provinces in which the Andes of Chile and Argentina are usually divided are shown in Fig. 3 (Mpodozis and Ramos 1989; Tassara and Yáñez 2003). South of 33–34°S, the Andes experiment a major change in morphology derived from the transition from a flat slab to a normal subduction segment. Consequently a broad mountain system converges in a narrower and lower system to the south formed from west to east by a Costal Cordillera corresponding to a Paleozoic block composed of metamorphic and magmatic rocks, a Central Valley mainly formed by Cenozoic to Quaternary depocenters, a Main Cordillera at the Chilean-Argentinian boundary where Mesozoic to Cenozoic strata are deformed, a Frontal Cordillera corresponding to a thick-skinned basement block and at the extran-Andean zone the San Rafael block with a surficial geology equivalent to the Frontal Cordillera. South of 39°S, the Patagonian Cordillera is cored by a Mesozoic batholith and at its northern section is associated with the Precordillera Patagónica where Paleozoic to Mesozoic rocks are exposed in the foreland area.

4 Structure of the Book

The second chapter analyzes from 30 to 55°S gravity and magnetic fields with the aim of understanding density and thermal structure of the Southern Andes and adjacent foreland region, working as an introductory chapter.

The third chapter analyzes the general U–Pb ages of the detrital components of the main sedimentary sections exposed through the different Andean segments. Thus, varying provenance sources through time are discussed, as well as Andean

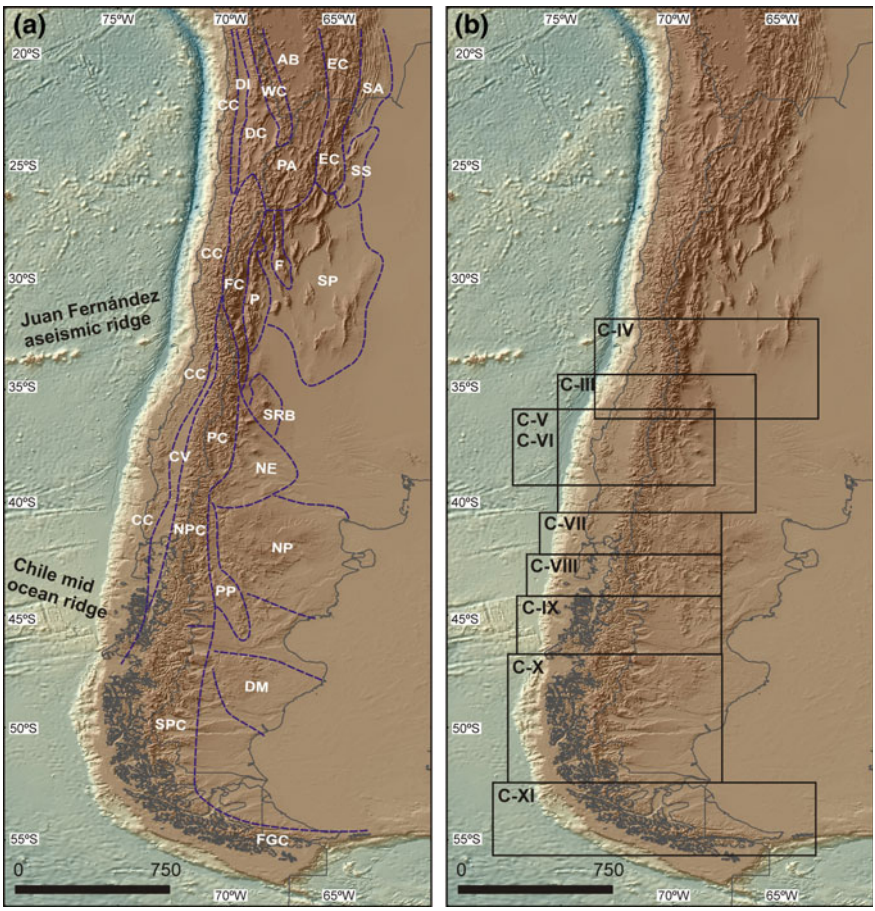

Fig. 3 *To the left* Main morphostructural provinces in which the Southern Andes are divided. *CC* Cordillera de la Costa, *DI* Depresión Intermedia, *DC* Cordillera de Domeyko, *WC* Cordillera Occidental; *PA* Puna; *AB* Altiplano Boliviano; *EC* Cordillera Oriental; *SA* Sierras Subandinas; *SS* Sistema de Santa Bárbara; *FC* Cordillera Frontal; *P* Precordillera; *F* Sistema de Famatina; *SP* Sierras Pampeanas; *CV* Valle Central; *PC* Cordillera Principal; *NE* Engolfamiento Neuquino; *SRB* Bloque de San Rafael; *NPC* Cordillera Norpatagónica; *PP* Precordillera Patagónica; *NP* Macizo Norpatagónico; *SPC* Cordillera Surpatagónica; *DM* Macizo del Deseado; *FGC* Cordillera Fueguina (based on Mpodozis and Ramos 1989; Tassara and Yáñez 2003). *To the right* Book structure (*empty rectangles* indicate areas analyzed in each chapter. The two initial chapters are focused in a regional perspective while the following eight analyze particular sectors of the Andes)

initiation uplift and exhumation based on changes on detrital compositions on the main sedimentary sections.

The fourth chapter is focused south of the present Pampean flat subduction segment, where a dramatic fall in altitude and amplitude in the Andean orogen is produced. Here, main growth stages as well as extensional periods interrupting Andean orogenesis are summarized.

The fifth chapter analyzes the structure and evolution of the area where the deepest and broadest part of the Neuquén embayment is incorporated into the orogenic wedge. The sixth chapter complements this through a detailed description of the development of the fold and thrust belt at 37°S, showing a complex evolutionary pattern that attends cycles of arc expansion and retraction.

The seventh chapter analyzes the segment at 39°S where the sag facies of the Neuquén embayment thin and consequently the structure changes to a narrow thick skinned system with a limited development to the foreland zone.

The eighth chapter focuses on the Cenozoic development of the Andes of North Patagonia and its relation to magmatic evolution, while the ninth chapter explores previous orogenic stages during the Late Cretaceous that show the cyclical character of the deformation.

The tenth chapter constitutes a review about the evolution and structure of the Southern Patagonian Andes and finally the eleventh chapter focuses on the Fueguian Andes at southernmost South America.

Acknowledgements The authors acknowledge Jorge Rabassa for the opportunity to show their research through this book.

References

Auboin JA (1973) Présentation de la Cordillère des Andes. Rev Géogr Phys Géol Dynam 15:5–10

Auboin JA, Borrello AV, Cecione G, Charrier R, Chotin P, Frutos J, Thiele R, Vicente JC (1973) Esquisse paleogeographique et structurale des Andes meridionales. Rev Géogr Phys Géol Dynam 15:11–71

Costa CH, Audemard MFA, Bezerra FHR, Lavenu A, Machette MN, París G (2006) An overview of the main Quaternary deformation of South America. Rev Asoc Geol Argentina 61:461–479

Gansser A (1973) Facts and theories on the Andes. J Geol Soc London 129:93–131

Mpodozis C, Ramos VA (1989) The Andes of Chile and Argentina. In: Ericksen GE, Cañas MT, Reinemud JA (eds) Geology of the Andes and Its Relation to Hydrocarbon and Mineral Resources Circumpacific Council for Energy and Mineral Resources, 11. Earth Science Series 59–90

Ramos VA (1999) Plate tectonic setting of the Andean Cordillera. Episodes 22(3):183–190

Ramos VA (2009) Anatomy and global context of the Andes: main geologic features and the Andean orogenic cycle. In: Kay SM, Ramos VA, Dickinson W (eds) Backbone of the Americas: Shallow Subduction, Plateau Uplift, and Ridge and Terrane Collision. Geological Society of America, Boulder, Memoir 204:31–65

Ramos VA (2010) The tectonic regime along the Andes: Present-day and Mesozoic regimes. Geol J 45:2–25

Russo RM, Silver PG (1994) Trench-parallel flow beneath the Nazca plate from seismic anisotropy. Science 263:1105–1111

Schellart WP, Freeman J, Stegman DR, Moresi L, May D (2007) Evolution and diversity of subduction zones controlled by slab width. Nature 446:308–311

Tassara A, Yáñez G (2003) Relación entre el espesor elástico de la litósfera y la segmentación tectónica del margen andino (15–47°S). Rev Geol de Chile 30(2):159–186

Density and Thermal Structure of the Southern Andes and Adjacent Foreland from 32° to 55°S Using Earth Gravity Field Models

Orlando Álvarez, Federico Lince Klinger, Mario Gimenez, Francisco Ruiz and Patricia Martinez

Abstract GOCE satellite data and EGM2008 model are used to calculate the gravity anomaly and the vertical gravity gradient, both corrected by the topographic effect, in order to delineate main tectonic features related to density variations. In particular, using the Bouguer anomaly from GOCE, we calculated the crust–mantle discontinuity obtaining elastic thicknesses in the frame of the isostatic lithospheric flexure model applying the convolution method approach. Results show substantial variations in the density, compositional and thermal structure, and isostatic and flexural behavior of the continental lithosphere along the Southern Andes and adjacent foreland region.

Keywords GOCE · EGM2008 · Isostasy · Density · Andes

1 Introduction

The study of the lithospheric structure related to density variations using gravimetric data has been improved in the past two decades. Since the early Earth gravity field models recovered from satellite orbit perturbation analysis to the last missions, specially designed for gravity information recovery such as GRACE (Gravity Recovery and Climatic Experiment) and GOCE (Gravity Field and Steady State Ocean Circulation Explorer), considerable improvements have been obtained. These satellite missions provide Earth gravity field models with increasing precision, resolution, and homogeneous coverage. The combination of data from

O. Álvarez (✉) · F. Lince Klinger · M. Gimenez · F. Ruiz · P. Martinez
Instituto Geofísico y Sismológico Ing. Volponi, Universidad Nacional de San Juan, Ruta 12-Km17, San Juan, Argentina
e-mail: orlando_a_p@yahoo.com.ar

O. Álvarez · F. Lince Klinger · M. Gimenez · P. Martinez
CONICET, Consejo Nacional de Investigaciones Cientifícas y Técnicas, Buenos Aires, Argentina

A. Folguera et al. (eds.), *Growth of the Southern Andes*,
Springer Earth System Sciences, DOI 10.1007/978-3-319-23060-3_2

different satellite missions leads to an excellent performance of both the long and short wavelengths of the gravimetric signal.

In particular, the model GO_CONS_GCF_2_DIR_R5 (Bruinsma et al. 2013) is a satellite-only model, based on a full combination of GOCE-SGG with GRACE and LAGEOS (LAser GEOdynamics Satellite). This model was obtained by the method of the direct approach , and is one of the maximum degree/order from satellite-only data (processing details are presented in Bruinsma et al. 2010; Pail et al. 2011). This allows obtaining a resolution of approximately $\lambda/2 \approx 2\pi R/N_{\max} \approx 66$ km with R being the mean Earth radius and $N_{\max} = 300$ the maximum degree and order of the harmonic expansion (Li 2001; Hofmann-Wellenhof and Moritz 2006; Barthelmes 2009).

Since the gravity field attenuates at high altitudes of satellite orbits, these satellites provide information only on the long wavelength part of the spectrum (Reguzzoni and Sampietro 2010). Thus, a way to improve the Earth gravity field model resolution is to incorporate terrestrial gravity data, as done in different models such as the EGM2008 (Pavlis et al. 2008, 2012) developed up to $N = 2190$ with $\lambda/2 = 9$ km, and EIGEN models from Förste et al. (2012) as EIGEN-6C4, also developed up to $N = 2190$ but including the last GOCE mission data. Despite its higher spatial resolution and global coverage, the disadvantage of these models is their inhomogeneous precision. For well-surveyed regions, where high quality terrestrial mean gravity anomalies are available, such as in North America, Europe, and Australia these models present geoid RMS-differences in the order of 4–6 cm (Yi and Rummel 2014). However, where surface gravity data are poor such as in South America, Africa, South-East Asia, and China regions, the RMS differences span between 20 and 38 cm (Yi and Rummel 2014).

The combined use of both kinds of models allow interpretation of medium-to-high (satellite-only models) and low (integrated models as EGM2008, EIGEN) wavelength anomalies related to crustal inhomogeneities. Nevertheless, a statistical comparison is needed between satellite-only and integrated models in order to estimate the error assessment prior to interpretation and analysis. Satellite only models ensure data quality, since these present homogeneous precision and no errors or sampling biases are present. Köther et al. (2012) explained that combined gravity models (such as EGM2008) can be used for density modeling of relatively smaller features such as shallower crustal structures, while satellite-only models are not appropriate for this purpose due to a lower spatial resolution.

Despite this, the homogeneous precision and regional coverage make them useful for regional studies, allowing interpretation of the gravity potential-derived signals at medium-to-high wavelengths (Braitenberg et al. 2011; Alvarez et al. 2012, 2014, 2015; Mariani et al. 2013; Li et al. 2013; Braitenberg 2014). In the present work, we use the satellite-only model from *GO_CONS_GCF_2_DIR_R5* (Bruinsma et al. 2013) to delineate the density and thermal structure of the Andes and adjacent foreland region from 32° to 55°S. In those regions, where the EGM2008 model (Pavlis et al. 2008, 2012) has an acceptable performance, density anomalies are interpreted as related to medium-to-low wavelengths.

2 Main Morphostructural Units of the Southern Andes

The northern analyzed region is located in the southern part of the Pampean flat slab zone. At these latitudes (32°S–33°S), the Andean structure is composed of a series of mountain ranges that comprises the Main Cordillera , the Frontal Cordillera, the southernmost region of the Precordillera, and the Sierras Pampeanas (Fig. 1; and see Chap. 1). The Frontal Cordillera is formed by a series of basement blocks that exposes Neo-Proterozoic to Paleozoic rocks, constituting the highest part of the fold and thrust belt at these latitudes (Ramos 1999). The Precordillera to the east is formed by thin- and thick-skinned imbricate fans, forming east-verging systems that expose Paleozoic to Triassic sequences, whose basal Laurentia-derived terms (Early Cambrian to Early Ordovician; Cuyania terrane; Fig. 1) were accreted to the Gondwana margin in Late Ordovician times (see Ramos 2004a, for a synthesis).

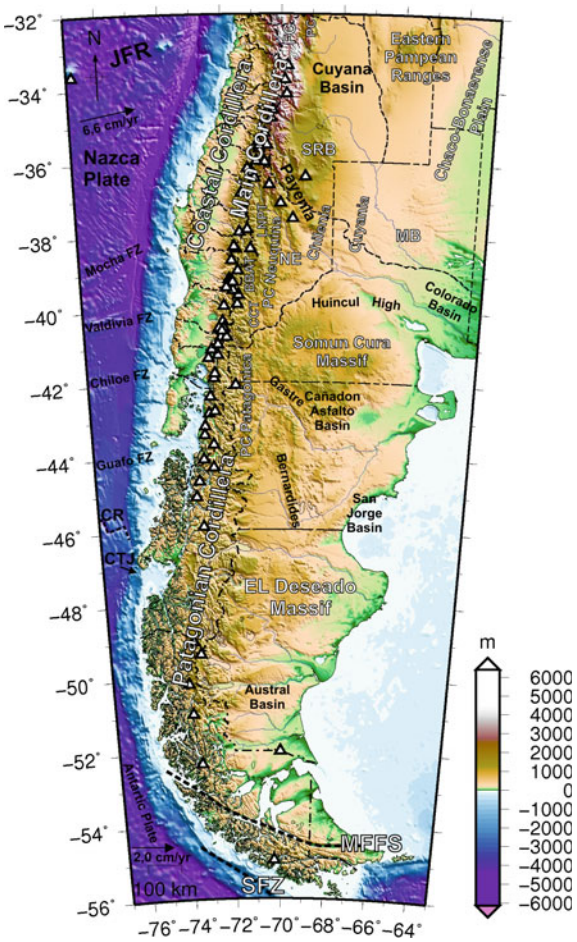

Fig. 1 Main morphostructural units mentioned in this chapter (*FC* Frontal Cordillera, *PC* Precordillera, *SRB* San Rafael Block, *NE* Neuquén Embayment, *MB* Mauidas Block, *LNPT* Loncopué Through, *BBAT* BíoBío Aluminé Through, *CCT* Collón Cura Through, *CR* Chile Rise, *CTJ* Chile Triple Junction). *MFFS* Magallanes Fagnano fault zone, *SFZ* Scotia fault zone. The Chilean–Argentinian border is indicated by a *dot* and *dashed line* and the coastal zone by a *solid black line*

Deformation in the Precordillera responsible for its present morphology occurred in the last 10 Ma, partly synchronous with the rise of the Pampean Ranges to the east in the foreland area (Jordan and Allmendinger 1986; Ramos et al. 2002). The thick-skinned Sierras Pampeanas constitute a set of Laramide-style basement blocks uplifted during the shallowing of the subducted Nazca Plate since late Miocene times (Ramos et al. 2002; Kay and Coira 2009). The NE region of the area under study comprises the Eastern Sierras Pampeanas that expose latest Proterozoic to Cambrian metamorphic rocks intruded by subduction-related to anorogenic magmatic rocks (Ramos 1988; Rapela et al. 1998; Lira et al. 1997). Late Miocene to Quaternary volcanic rocks unconformably overlying the Proterozoic to Paleozoic basement at the foreland area indicate the eastern migration of the volcanic arc during the flattening of the Nazca Plate in the last 17 Ma (Brogioni 1990; Kay and Gordillo 1994).

South of this region (−35°S), the Payenia volcanic zone is characterized by mainly Quaternary extensive volcanic fields, located in the back-arc zone. These young volcanic rocks overly Paleozoic to Cenozoic rocks and more locally, Mesozoic sedimentary sections of the Neuquén embayment. The Neuquén embayment is segmented by basement structures with N-to-NW structures and more locally by the Huincul Ridge, a transverse-to-the Andes regional lineament (see Ramos 1999 and references therein), corresponding to a first order structural feature (Turner and Baldis 1978), interpreted in some works as the extensional reactivation of the northern limit of the Patagonia Paleozoic terrane (Ramos et al. 2004b). North of this, the Mahuidas basement block is constituted by Precambrian metamorphic rocks intruded by Paleozoic plutonic rocks (Linares et al. 1980).

The Patagonian Cordillera to the south, a relatively narrow mountain system compared with the Central Andes to the north, is characterized by a continuous Mesozoic to Cenozoic batholith emplaced along the western slope and axial zone of the Andes, from nearly 39°S to about 52°S (Hervé et al. 2004). A strike-slip crustal structure, the Liquiñe–Ofqui fault zone (LOFZ) (Fig. 1) (Hervé et al. 1996; Cembrano et al. 1996, among others) crosses the axial part of the Northern Patagonian Andes, controlling the emplacement of the volcanic arc corresponding to the Southern Volcanic Zone (see Ramos 2009 and references therein).

Two basement-foreland cores characterize the extra-Andean region, the Somuncura Massif (Windhausen 1931) and the Deseado Massif. The central zone of these foreland Paleozoic cores is partly covered by siliceous Jurassic rocks associated with widespread synextensional volcanic activity during Pangea breakup (Uliana et al. 1985; Alric et al. 1996; Feraud et al. 1999; Ghidella et al. 2002; Ramos 2004b). These foreland cores are flanked by Mesozoic extensional basins such as Cañadón Asfalto, Río Mayo, Austral, and San Jorge Gulf basins (Fig. 1). The Precordillera Patagonica across the Patagonian foreland zone constitutes a feature separated from the Andes to the west that results from the partial inversion of these extensional basins (Ramos 1999).

3 The Topography-Reduced Gravity Anomaly (Ga)

The observed potential is obtained from the Earth gravity field model. The disturbing potential (T) is calculated subtracting the potential field from the reference ellipsoid (WGS84) (Janak and Sprlak 2006). This disturbing potential allows calculation of different derived quantities, related to crustal density heterogeneities. The topography reduced gravity anomaly $(\Delta_{g_{tr}})$ is the difference between the real gravity (g) at a given point (h, λ, ϕ), and the gravity of the reference ellipsoid (γ) at the same coordinates, but at the ellipsoidal height h-ζ_g (where ζ_g is the generalized height anomaly) and without considering the effect of the topographic masses above the geoid (g_t) (Molodensky et al. 1962; Hofmann-Wellenhof and Moritz 2006; Barthelmes 2009). The height h is assumed on or above the Earth surface ($h \geq h_t$). Thus, the measured gravity at the Earth surface can be used for calculation of the gravity anomaly, in the modern definition, without downward continuation or any reduction as it is a function in the space outside the masses (Barthelmes 2009).

$$\Delta_{g_{tr}}(h, \lambda, \phi) = g(h, \lambda, \phi) - g_t(h, \lambda, \phi) - \gamma\left(h - \zeta_g, \lambda, \phi\right) \quad (1)$$

For calculation of the gravity anomalies (Janak and Sprlak 2006), we used the model of GOCE *GO_CONS_GCF_2_DIR_R5* (Bruinsma et al. 2013) up to its maximum degree/order = 300 (Fig. 2), and the EGM2008 (Pavlis et al. 2008, 2012) up to degree/order = 2159 (Fig. 3). For an approximate calculation of the effect of the topographic masses, we used a global relief model which includes ocean bathymetry (ETOPO1, Amante and Eakins 2009) and a mass density distribution hypothesis. We utilized standard densities of 2670 kg/cm^3 for continental crust and a density of 1030 kg/cm^3 for the sea. The topographic effect was calculated at a height of 7000 m to ensure that all values are above the topography and in a spherical coordinate system. The topographic elements were approximated using spherical prisms or Tesseroids (Uieda et al. 2010; Alvarez et al. 2013) taking into account the Earth curvature in order to avoid the error introduced when using a planar approximation (Grombein et al. 2013; Bouman et al. 2013). All calculations were carried out with respect to the system WGS84 on a regular grid of 0.05° grid cell size. These topography corrected gravity anomalies are useful for highlighting the effects of different rock densities into the crust, geological structures and basins.

4 The Topography Corrected Vertical Gravity Gradient (Tzz)

The gravity gradient tensor (Marussi tensor) is obtained as the second derivative of the disturbing potential T (e.g., Hoffman-Wellenhof and Moritz 2006) and is composed of five independent elements. The Marussi tensor components M = T_{ij} can be expressed and solved numerically in a spherical coordinate system

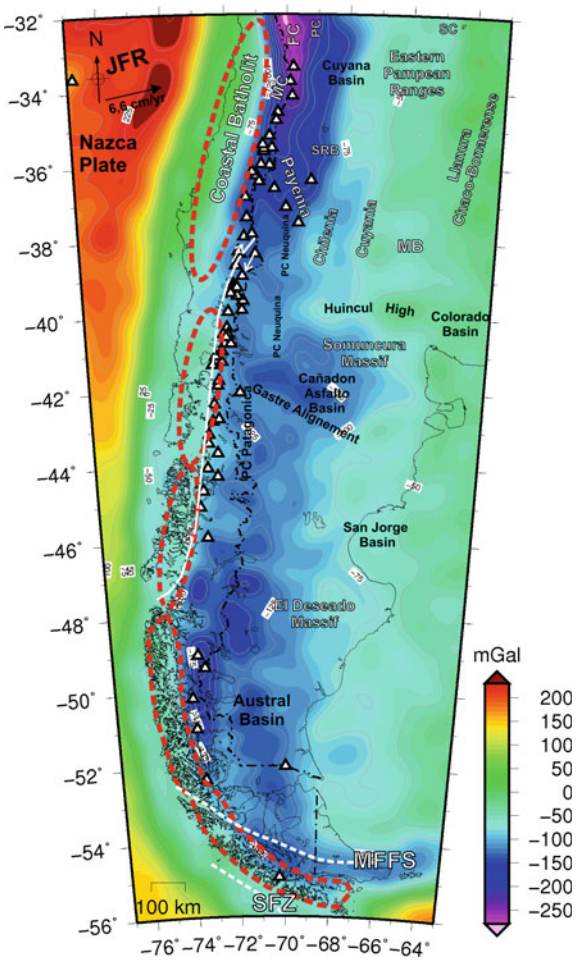

Fig. 2 Gravity anomaly from GOCE model GO_CONS_GCF_2_DIR_R5 (Bruinsma et al. 2013) corrected by the topographic effect (*FC* Frontal Cordillera, *PC* Precordillera, *SC* Sierras de Cordoba, *MC* Main Cordillera, *SRB* San Rafael Block, *MB* Mahuidas Block, and *JFR* Juan Fernandez Ridge). *Thin White dashed line* represents the Liquiñe Ofqui fault zone, *MFFS* Magallanes Fagnano fault zone, *SFZ* Scotia fault zone. The Chilean–Argentinian border is indicated by a *dot* and *dashed line* and the coastal zone by a *solid black line*

(Tscherning 1976; Rummel et al. 2011). The vertical gravity (Tzz) gradient is the second radial derivative of the disturbance potential T.

$$T_{zz} = \frac{\partial^2 T}{\partial r^2} \left[1\text{Eötvös} = 10^{-4} \frac{\text{mGal}}{\text{m}} \right] \tag{2}$$

The vertical gravity gradient highlights superficial density anomalies and allows delineating the location of an anomalous mass with better detail and accuracy than the gravity anomaly itself (Braitenberg et al. 2011). Since the Tzz is a derivative of gravity, the spectral power of gravity gradient signals is pushed to higher frequencies, resulting in a signal more focalized to the source than the gravity anomaly (Li 2001). Therefore Tzz is better for detection of the edge of geological structures and to distinguish the signal due to a smaller superficial density variation from an

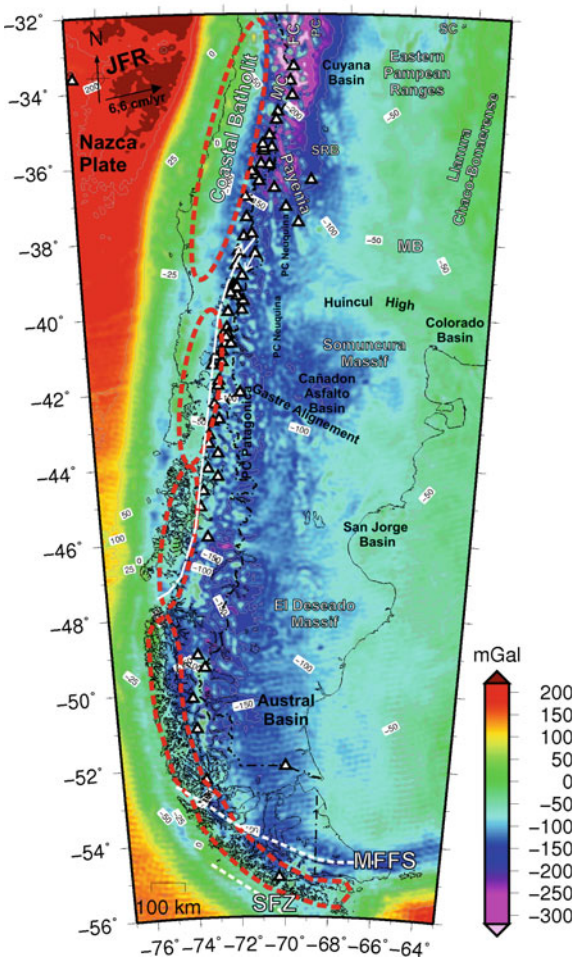

Fig. 3 Gravity anomaly from EGM2008 model (Pavlis et al. 2008, 2012) corrected by the topographic effect

extensive deeper mass, being the *Ga* more sensitive to regional signals and deeper sources (Alvarez et al. 2012). Relative denser bodies are related to a positive gradient value while a negative gradient is related to less dense bodies. Abrupt changes may indicate a high-density contrast between two different lithologies.

We calculated the vertical gravity gradient from GOCE *GO_CONS_GCF_2_DIR_R5* (Bruinsma et al. 2013) in a geocentric spherical coordinate system at the calculation height of 7000 m to ensure that all values were above the topography (Fig. 4) and also for the EGM2008 model (Fig. 5). The values were calculated on a regular grid with a cell size of 0.05°, with the maximum degree and order of the harmonic expansion ($N = 300$, $N = 2159$) for each model. The topographic effect was removed from the fields in order to eliminate the correlation with the topography (Alvarez et al. 2013) as made for the gravity anomaly. The topographic correction amounts up to tens of Eötvös for the *Tzz*, becoming higher over the

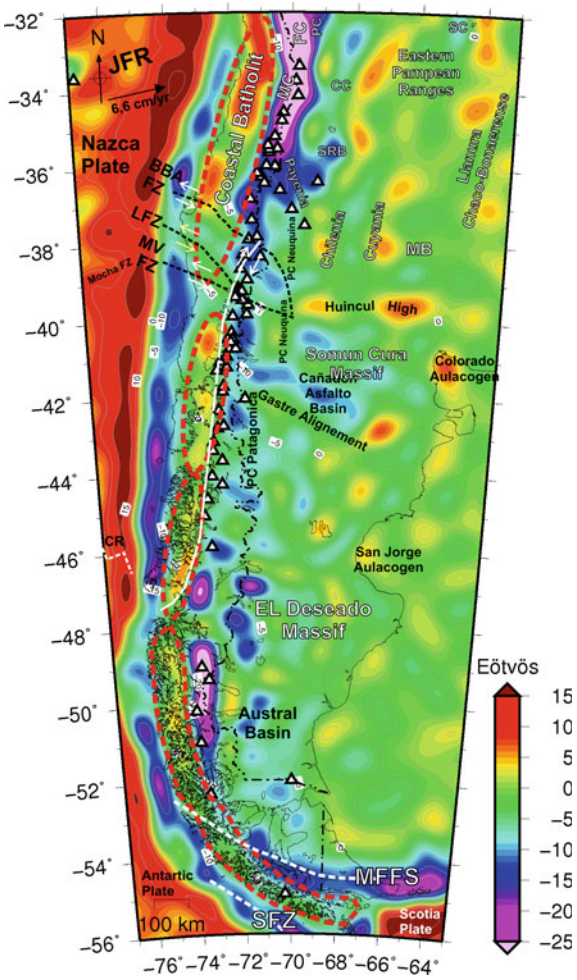

Fig. 4 Vertical gravity gradient from GOCE model GO_CONS_GCF_2_DIR_R5 (Bruinsma et al. 2013) corrected by the topographic effect (*BBAFZ* BioBio Alumine fault zone, *LFZ* Lanalhue fault zone, *MVFZ* Mocha Villarica fault zone, *MFFS* Magallanes Fagnano fault zone, *SFZ* Scotia fault zone)

maximum topographic elevations (e.g., the Main Andes) and lower over the topographic depressions such as the Chilean Trench.

After a statistical analysis and considering the sparseness of terrestrial data in the region under study (Pavlis et al. 2008, 2012), the most reliable areas to apply the EGM2008 model are mainly offshore and forearc regions comprised between 36° and 48°S. Thus, the GOCE model (TIM_R5) becomes more appropriate than the EGM2008 model in the region under study despite its lower resolution (but homogeneous precision). Results obtained by means of the EGM2008 model will only be analyzed and compared to GOCE in the regions of higher performance, in order to solve the different anomalies in greater detail. The combined use of both models, considering their best individual qualities, has been already tested in different studies (Braitenberg et al. 2011; Alvarez et al. 2012, 2014, 2015).

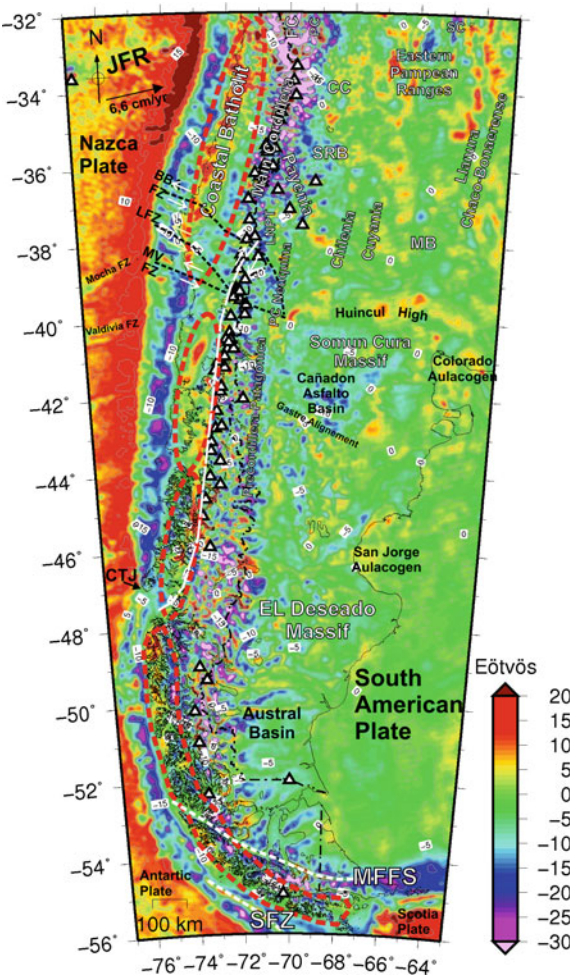

Fig. 5 Vertical gravity gradient from EGM2008 model (Pavlis et al. 2008, 2012) corrected by topographic effect. *CTJ* Chile triple junction

5 Isostatic Modeling

Isostatic theory explains the elastic behavior of the lithosphere, describing the effect of the inhomogeneous distribution of the crustal loads. The Airy model considers that different cortical sections behave in hydrostatic equilibrium, constituting a "topographic load" compensated by a "crustal root"

$$\Delta R = \frac{\sigma}{\sigma_1 - \sigma} h \tag{3}$$

where σ is the crustal density, σ_1 is the mantle density, ΔR: the crustal root or compensation and h is the topography. As this expression indicates, crustal and

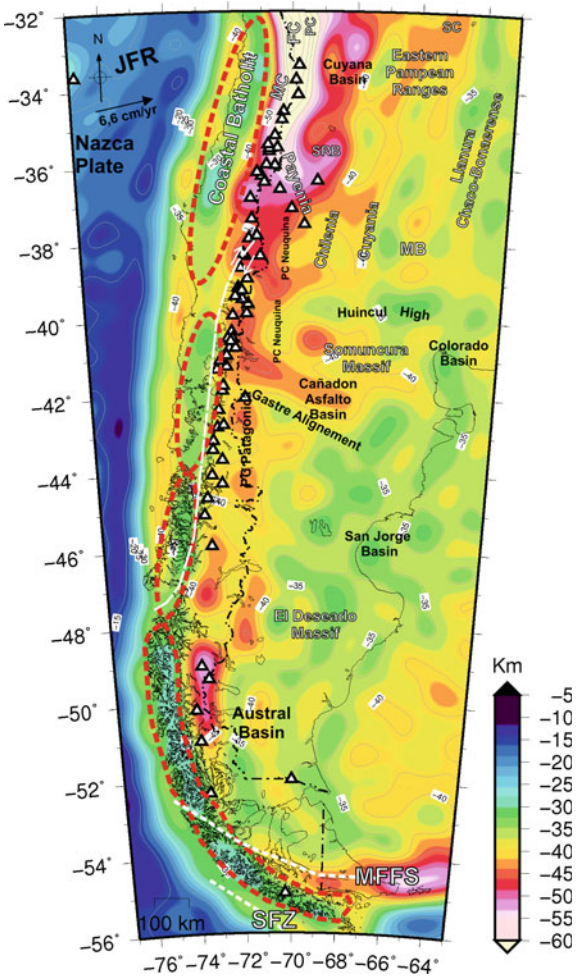

Fig. 6 Moho from GOCE model GO_CONS_GCF_2_DIR_R5 (Bruinsma et al. 2013) obtained from inversion of the Bouguer anomaly

mantle densities remain constant and consequently the depth of compensation varies in function of the topography. For calculation of the Airy response we considered a crust–mantle density contrast of 400 kg/cm^3 and the relief model ETOPO1.

Then, we obtained the depth to the crust–mantle interface (Hydrostatic Moho) by using Eq. (3), taking into account as normal crustal thickness Tn = 35 km. This Moho was then compared (by subtracting) to the crust–mantle interface (Fig. 6) obtained by inversion of the Bouguer anomaly (Fig. 2) calculated from the GOCE model *GO_CONS_GCF_2_DIR_R5* (Bruinsma et al. 2013). Near to zero values of this "residual" Moho (Fig. 7) indicates different regions that are near the isostatic equilibrium or that behave as compensated by a crustal root, while negative values indicate an overcompensation (the crustal root obtained by means of the Bouguer

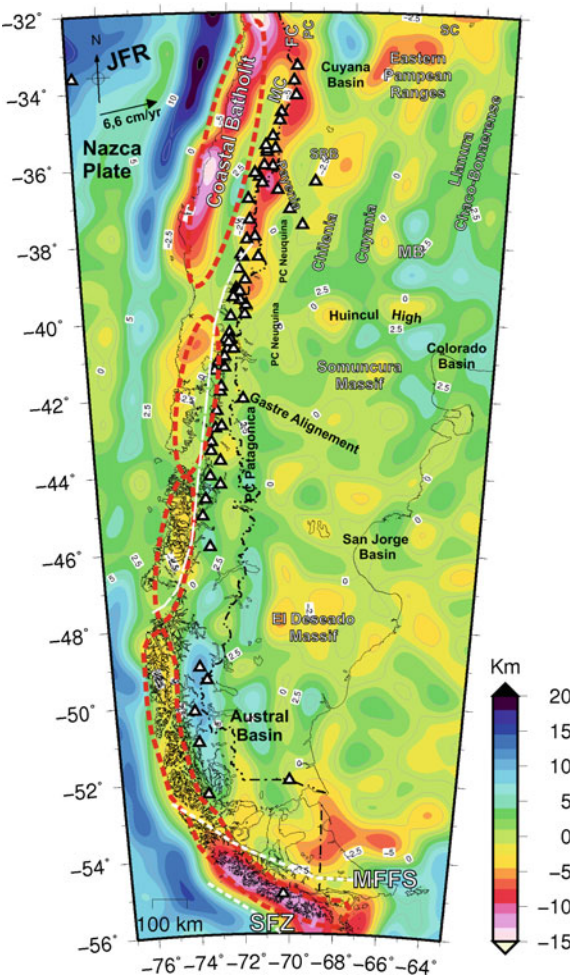

Fig. 7 Residual between the isostatic Moho (Airy) and Moho obtained by inversion of the Bouguer anomaly from GOCE model GO_CONS_GCF_2_DIR_R5 (Bruinsma et al. 2013). Near zero values indicates a hidrostatic balance, while negative values indicate an overcompensation of the crustal root and positive ones the expression of a deficiency in isostatic compensation

anomaly is deeper than the one obtained following the Airy hypothesis), and positive values indicate an undercompensation, i.e., the crustal root is not deep enough to compensate the topographic loads.

6 Effective Elastic Thickness

The compensation of the topographic masses is approximated through the Airy theoretical model that considers a local compensation and the Vening Meinesz model that indicates that the compensation is performed by a regional bending of

the plate, which best describes the mechanical behavior and stress state of a loaded lithosphere (Introcaso 2006).

The thickness and viscosity of the lithosphere, or lithospheric strength, is related to the thermal state, rheological and compositional properties of the crust and is well characterized by the flexural rigidity (Lowry et al. 2000). The last can be interpreted in terms of the elastic thickness (*Te*) by making some assumptions regarding the Young modulus and the Poisson ratio. *Te* defines the maximum size and wavelength of the surface loading that can be supported without an elastic break of the lithosphere. The flexural rigidity *D* can be expressed by:

$$D = T_e^3 \cdot \frac{E}{12(1 - v^2)} \tag{4}$$

where E = 100 GPA = 10^{11} N/m^2 is the Young's modulus, and v = 0.25 is the Poisson's ratio. The isostatic state and deformation of the upper crust are reflected in the spatial distribution of the *Te*, whose variation can be explained by heat flow distribution and a change in the Young modulus. A relation between *Te* and the geometry and composition of the flexured plate, external forces and the thermal structure has been reported by different authors (e.g., Göetze and Evans 1979; Lyon-Caen and Molnar 1983; Burov and Diament 1995; Hackney et al. 2006).

Different methods have been developed for estimation of the elastic thickness, as the flexural coherence analysis, the spectral methods, and the convolution approach (Braitenberg et al. 2002; Wienecke 2006). The last has the advantage of being a method of double entry that calculates the flexure parameters by the best fit of the observed crust–mantle interface obtained by gravity inversion and a crust–mantle interface computed due to a flexure model see Fig. 8 (www.lithoflex.org) (Wienecke 2006; Wienecke et al. 2007; Braitenberg et al. 2007). Isostatic modeling adopts the isostatic thin plate flexure model (e.g., Watts 2001). To estimate the elastic properties of the plate for a known load are needed a crustal load (combination of the overlying topography plus a density model) and the crust–mantle interface to be used as a reference surface (Wienecke 2006).

The topographic load was calculated using topographic/bathymetric data from ETOPO1 (Amante and Eakins 2009). The densities used for calculation were 1030 kg/m^3 for water and 2800 kg/m^3 for the crust. The undulating boundary corresponding to the Moho was calculated by gravity inversion of the Bouguer anomaly field (from GOCE *GO_CONS_GCF_2_DIR_R5*, http://icgem.gfz-potsdam.de/ICGEM/, Bruinsma et al. 2013). This method requires two input parameters, the density contrast (400 kg/m^3) and reference depth or normal crustal thickness (Tn = 35 km) (values between 30 and 40 km have been adopted in numerous works as normal crustal thickness).

The flexural rigidity was inverted in order to match the known loads with the known crustal thickness model (i.e., to model the gravity Moho in terms of an isostatic model). The elastic thickness was allowed varying in the range of 1< *Te* <